Statistics of baryon isocurvature perturbations in the inflationary universe

Kazuhiro Yamamoto
Uji Research Center, Yukawa Institute for Theoretical Physics, Kyoto University, Uji 611, Japan and Department of Physics, Hiroshima University, Higashi-Hiroshima 724, Japan

Michiyasu Nagasawa
Department of Physics, University of Tokyo, Bunkyo, Tokyo 113, Japan

Misao Sasaki
Department of Physics, Kyoto University, Kyoto 606, Japan

Hiroshi Suzuki
Department of Physics, Tohoku University, Sendai 980, Japan

Jun' ichi Yokoyama
Uji Research Center, Yukawa Institute for Theoretical Physics, Kyoto University, Uji 611, Japan
(Received 5 May 1992)

The statistical distribution of baryon-number fluctuations, which may provide a proper initial condition for the minimal isocurvature scenario, is carefully investigated both analytically and numerically. For fluctuations associated with power-law inflation, we find that the distribution is highly non-Gaussian on scales of pregalactic star formation while it is Gaussian on scales of large-scale structure. On the other hand, in the pure de Sitter universe, it is shown to be Gaussian on any astrophysical scale. It is also discussed why the Gaussian nature appears in these models.

PACS number(s): 98.80.Cq, 98.60.Ac

I. INTRODUCTION

One of the most important problems in cosmology is to explain how the observed cosmic structure was formed. Many ideas have been proposed on the origin of large-scale structure. Unfortunately, however, we have been unable to single out the correct model among them due to the lack of accurate observational data that should determine the fundamental parameters, such as the Hubble parameter, the density parameter, or the cosmological constant, not to mention the main ingredient of matter contents. In this situation, taking both merits and demerits of each scenario into account, Peebles and Silk [1] concluded that the cold-dark-matter scenario in the inflationary cosmology [2] and the minimal baryon isocurvature scenario in a low-density universe surpass other candidates at present.

The initial condition for the standard cold-dark-matter scenario is an adiabatic fluctuation with a scale-invariant spectrum that is predicted by typical inflationary models. Although its initial condition is well motivated, it assumes artificial biasing, whose physical mechanism is yet unclear, in the process of galaxy formation. Moreover, this scenario has other serious difficulties such as too large velocity dispersion on small scales [3]. It is also difficult to reproduce very-large-scale structure on scales over 100 Mpc [4] without contradiction to the observed anisotropy of the cosmic microwave background (CMB) radiation on the large scale [5].

On the other hand, the minimal isocurvature scenario [6] proposed by Peebles attempts to explain structure formation on a purely phenomenological basis in a low-density universe, which is supported by recent observations [7]. Such a low-density universe may be dominated by baryonic matter since $\Omega_0 \sim 0.1$ is marginally consistent with the value allowed by the primordial nucleosynthesis argument [8]. This scenario is attractive because the cosmic structure is formed only by the matter whose existence we know, i.e., the baryon and the radiation. However, it assumes very *ad hoc* initial density fluctuations, namely, isocurvature fluctuations with a steep spectrum. Having less power on large scales, this scenario can be consistent with the observed large-angle isotropy of CMB [9]. On small scales, the large amplitude of isocurvature fluctuation allows star formation soon after the recombination of matter. Presumably these stars reionized the medium in the universe and as a result the small-angle anisotropy of CMB was smoothed out through diffusion in the plasma, though the reionization mechanism is not well analyzed. Still more, a nice feature of large-scale coherence in the peculiar velocity field can be obtained [10,11]. In this way, the minimal isocurvature scenario seems successful.

Recently, Yokoyama and Suto [10] and Sasaki and Yokoyama [12] have shown that it is possible to provide the baryon isocurvature fluctuations with a spectrum appropriate for the minimal isocurvature scenario in the context of inflationary cosmology, based on a mechanism of baryogenesis in which baryon-number fluctuations are generated through the soft *CP* violation induced by a spa-

tially varying pseudo Goldstone field [15]. We note that a low-density universe is compatible with inflation if the cosmological constant is nonvanishing. In particular, Sasaki and Yokoyama [12] have presented a rigorous expression for the baryon power spectrum in the power-law inflationary background [13,14]. In their model the pseudo Goldstone field is identified with the Majoron field associated with a heavy Majorana lepton. The coherent Majoron field is generated in the inflationary era. The spectrum of the baryon-number fluctuation was found to be almost scale invariant on small scales and white-noise-type on large scales, which is exactly what one needs for the minimal isocurvature scenario.

In general the adiabatic density fluctuation induced by the inflaton field has a Gaussian random-phase distribution. On the other hand the baryon-number fluctuation predicted in [10,12] has a non-Gaussian nature because it is given by a sinusoidal projection of a Gaussian probability variable. This may have significant cosmological implications.

In this paper, we investigate the property of the baryon-number fluctuation by using both analytical and numerical methods. In particular, we simulate its probability distribution on various scales in both configuration and Fourier spaces using the Monte Carlo method. To do this we consider not only a fully three-dimensional model but also a one-dimensional model that reproduces all the essential properties in the original theory such as correlation functions, since the latter allows a large enough dynamic range of scales.

The rest of the paper is organized as follows. In Sec. II, we review the previous results on the baryon-number fluctuation generated through the aforementioned mechanism. A detailed study of the probability distribution of the baryon-number fluctuation in the power-law inflationary background is described in Sec. III. The case of pure de Sitter inflation is described in Sec. IV. Section V is devoted to discussion and the conclusion.

II. POWER SPECTRUM OF THE BARYON-NUMBER FLUCTUATION

Following [12], we consider the baryon-number fluctuation given by

$$B(x)=B_*\sin\left[\frac{A(x)}{f}\right], \tag{2.1}$$

where $A(x)$ is the Majoran field and f is its associated mass scale. Assuming $A(x)$ to be an effectively massless free field by imposing some symmetry, one may express the power spectra of baryon-number fluctuations in terms of the two-point correlation function of $A(x)$. In particular, in the case of pure de Sitter background or power-law inflationary background, the expression may be analytically evaluated. We review these results [10,12,16] briefly.

The metric of pure de Sitter space time may be expressed as

$$ds^2=-dt^2+a(t)^2dx^2, \tag{2.2}$$

where $a(t)=e^{Ht}$ is the scale factor with H being the Hubble parameter. The free field $A(x)$ is decomposed as

$$A(x,\eta)=\int\frac{d^3k}{(2\pi)^{3/2}}[\hat{a}_k A_k(\eta)\exp(ikx) +\hat{a}_k^{\dagger}A_k(\eta)^*\exp(-ikx)], \tag{2.3}$$

where $\hat{a}_k$ and $\hat{a}_k^{\dagger}$ are the annihilation and creation operators, respectively, and we have introduced the conformal time η, defined by $d\eta=dt/a(t)$. The mode function $A_k(\eta)$ is determined from the field equation in the expanding background, and it can be solved under a suitable boundary condition

$$A_k(\eta)=\left[\frac{\pi}{4}\right]^{1/2}H(-\eta)^{3/2}H^{(1)}_{3/2}(-k\eta)\simeq -i\frac{H}{\sqrt{2}k^{3/2}}, \tag{2.4}$$

where $H^{(1)}_{3/2}$ is the (3/2)th Hankel function of the first kind and the last approximation is justified if $-k\eta\ll 1$. The equal-time two-point correlation function of $A(x)$ is given by

$$\langle A(r,\eta)A(0,\eta)/f^2\rangle =\int_{k_{\rm IR}<k<k_{\rm UV}}\frac{d^3k}{(2\pi)^3}|A_k(\eta)|^2\exp(ikr)/f^2 \simeq 2\beta\ln\left[\frac{1}{k_{\rm IR}|r|}\right], \tag{2.5}$$

where $k_{\rm IR}$ is an infrared cutoff, $k_{\rm UV}$ is an ultraviolet cutoff which corresponds to the horizon scale, and $\beta\equiv H^2/8\pi^2f^2$. Following the prescription in [12] (see also Appendix A), we can get the two-point correlation function of $B(x)$ as

$$\langle B(r,\eta)B(0,\eta)\rangle=\frac{B_*^2}{2}\left[\frac{1}{a(\eta)H|r|}\right]^{2\beta}. \tag{2.6}$$

Then the power spectrum of $B(x)$ is given by

$$P_B(k,\eta):=\int d^3r\langle B(r,\eta)B(0,\eta)\rangle e^{-ikr} =\frac{2\pi B_*^2}{k^3}\left[\frac{k}{aH}\right]^{2\beta}\frac{\sin(1-\beta)\pi}{2(1-\beta)}\Gamma(3-2\beta) \simeq(2\pi)^3\frac{B_*^2}{4\pi}\frac{\beta}{k^3}\left[\frac{k}{aH}\right]^{2\beta}\quad(\text{for }\beta\ll 1). \tag{2.7}$$

Thus it has no characteristic scale except the horizon size.

On the other hand, in power-law inflation, the metric is given by (2.2) with the scale factor proportional to t^{1+n} $(n>0)$. In terms of the conformal time η, the scale factor and the time-dependent Hubble parameter are expressed as

$$a(\eta)=\frac{1}{(-H_*\eta)^{1+1/n}}, \qquad H(\eta)=\left[1+\frac{1}{n}\right]H_*(-H_*\eta)^{1/n}, \tag{2.8}$$

where H_* is a constant, and the mode function $A_k(\eta)$ as

$$A_k(\eta)=\left[\frac{\pi}{4}\right]^{1/2}H(\eta)(-\eta)^{3/2}H^{(1)}_{3/2+1/n}(-k\eta)$$
$$\simeq\frac{H(\eta)}{\sqrt{2}k^{3/2}}\left[\frac{1}{-k\eta}\right]^{1/n}\simeq\frac{H_*^{1+1/n}}{\sqrt{2}k^{3/2+1/n}}\,, \tag{2.9}$$

where we have assumed $n\gg1$. The two-point correlation function of $A(x)$ is then expressed as

$$\langle A(r,\eta)A(0,\eta)/f^2\rangle\simeq n\beta(\eta)\left[\left[\frac{r_0^2}{\eta^2}\right]^{1/n}-\left[\frac{r^2}{\eta^2}\right]^{1/n}\right], \tag{2.10}$$

where r_0 corresponds to the infrared cutoff $k_{\rm IR}^{-1}$ and $|\eta|$ to the ultraviolet cutoff $k_{\rm UV}^{-1}$, which is essentially equal to the horizon scale. Similar to the case of pure de Sitter background, $\beta(\eta)$ is defined by $\beta(\eta):=H^2(\eta)/8\pi^2f^2$. The expectation value $\langle A(0,\eta)^2\rangle$ is regularized at the horizon scale as

$$\langle A(0,\eta)^2/f^2\rangle\simeq n\beta(\eta)\left[\left[\frac{r_0^2}{\eta^2}\right]^{1/n}-1\right]. \tag{2.11}$$

Note that we are interested in the range $n\beta(\eta)\lesssim1$ from the cosmological point of view [12,16]. The same procedure in the pure de Sitter background can be used to find the power spectrum of the baryon-number fluctuations. The two-point correlation function of $B(x)$ and its spectrum are expressed as

$$\langle B(r,\eta)B(0,\eta)\rangle=\frac{B_*^2}{2}\exp\left\{n\beta(\eta)\left[1-\left[\frac{r^2}{\eta^2}\right]^{1/n}\right]\right\} \tag{2.12}$$

and

$$P_B(k,\eta)=\frac{2\pi B_*^2}{k^3}e^{n\beta(\eta)}\int_0^\infty ds\,s\sin s\exp\left[-\left[\frac{k_c}{k}s\right]^{2/n}\right]$$
$$=:\frac{2\pi B_*^2}{k^3}e^{n\beta(\eta)}J(n,k)\,, \tag{2.13}$$

where $k_c:=[n\beta(\eta)]^{n/2}/|\eta|$. The function $J(n,k)$ has different asymptotic forms on the different sides of k_c, and the power spectrum $P_B(k,\eta)$ takes the following form in the two asymptotic regions:

$$P_B(k)\simeq\begin{cases}\dfrac{\pi^2B_*^2}{nk^3}e^{n\beta(\eta)}\left[\dfrac{k}{k_c}\right]^{-2/n} & \text{for } k\gg k_c,\\[2ex] \dfrac{\pi B_*^2}{k_c^3}e^{n\beta(\eta)}\left[\dfrac{n\pi}{3}\right]^{1/2}\left[\dfrac{3n}{2e}\right]^{3n/2} & \text{for } k\ll k_c\,,\end{cases} \tag{2.14}$$

Thus on the small scale ($k\gg k_c$) the spectrum of fluctuations is almost scale invariant, while on the large scale ($k\ll k_c$) it is white noise. As discussed in [12], the power-law index of $n\simeq10\sim20$ may provide an appropriate initial condition for the minimal isocurvature scenario.

III. PROBABILITY DISTRIBUTION IN POWER-LAW INFLATION

A. Analytic properties

First we consider a pointwise probability distribution of $B(x)$. The probability distribution of $A(x)$ at a given spatial point $\rho(A(x))$ is Gaussian with the average equal to zero and the variance equal to $\langle A(x)^2\rangle$. The probability distribution of $B(x)$ at a given spatial point $\rho(B(x))$ is given by

$$\rho(B(x))=\int_{-\infty}^{\infty}dA\frac{\exp[-A^2/2\langle A(x)^2\rangle]}{[2\pi\langle A(x)^2\rangle]^{1/2}}\delta(B_*\sin(A/f)-B(x))$$
$$=\frac{1}{[B_*^2-B(x)^2]^{1/2}[2\pi\langle A(x)^2/f^2\rangle]^{1/2}}\sum_{n\in Z}\exp(-\{(-1)^n\arcsin[B(x)/B_*]+n\pi\}^2/2\langle A(x)^2/f^2\rangle)\,, \tag{3.1}$$

where we have used an identity $\delta(g(x))=\sum_n\delta(x-x_n)/|g'(x_n)|$ with x_n's being the zeros of $g(x)$. Since Eq. (2.11) is rewritten as

$$\langle A(x)^2/f^2\rangle\simeq\left[\frac{k_c}{k_{\rm IR}}\right]^{2/n}, \tag{3.2}$$

we find $\langle A(x)^2/f^2\rangle\gg1$. In this limit, the summation of n in Eq. (3.1) can be approximated by an integral to yield

$$\rho(B(x))=\frac{1}{\pi[B_*^2-B(x)^2]^{1/2}}\,, \tag{3.3}$$

which has sharp peaks at $B(x)=\pm B_*$. Thus the probability distribution of $B(x)$ at a given spatial point differs substantially from a Gaussian distribution.

The distribution derived above describes the property of the fluctuation at a single spatial point that disregards the correlation in the neighborhood of the point. In order to investigate the spatial correlation, one needs to know the statistical properties of the Fourier transform of $B(x), B_k$.

For small scale ($k \gg k_c$), we may separate the long- and short-wavelength parts of $A(x)$ as

$$A(x,\eta)=\int_{k_{\rm IR}<|k|\le k_s}\frac{d^3k}{(2\pi)^{3/2}}[\hat{a}_k A_k(\eta)\exp(ikx)+\text{H.c.}]+\int_{k_s<|k|<k_{\rm UV}}\frac{d^3k}{(2\pi)^{3/2}}[\hat{a}_k A_k(\eta)\exp(ikx)+\text{H.c.}]$$
$$=:A(x)_L+A(x)_S\ , \tag{3.4}$$

where k_s is an arbitrary scale with $k_s \gg k_c$. Since Eqs. (2.11) and (3.2) yield $\langle A(x)_S^2/f^2\rangle \simeq (k_c/k_s)^{2/n} \ll 1$, $B(x)$ may be expanded as

$$B(x)=B_*\sin\left[\frac{A(x)_L}{f}+\frac{A(x)_S}{f}\right]=B_*\sin\left[\frac{A(x)_L}{f}\right]\cos\left[\frac{A(x)_S}{f}\right]+B_*\cos\left[\frac{A(x)_L}{f}\right]\sin\left[\frac{A(x)_S}{f}\right]$$
$$\simeq B_*\sin\left[\frac{A(x)_L}{f}\right]+B_*\frac{A(x)_S}{f}\cos\left[\frac{A(x)_L}{f}\right]=:B(x)_L+B(x)_S\ , \tag{3.5}$$

where $B(x)_S$ is regarded as a small-scale fluctuation around a large-scale background value $B(x)_L$. The spatial variation of $A(x)_L/f$ over the scale $1/k_s$ is estimated by the expectation value

$$\left\langle\left[\frac{dA_L}{dx}\frac{1}{k_s}\right]^2\Big/f^2\right\rangle=\int_{k_{\rm IR}<|k|<k_s}\frac{d^3k}{(2\pi)^3}\frac{|A_k|^2}{f^2}\frac{k^2}{k_s^2}$$
$$=\frac{1}{n}\left[\frac{k_c}{k_s}\right]^{2/n}\ll 1\ , \tag{3.6}$$

while the distribution of $B(x)_L$ itself is highly non-Gaussian as given by Eq. (3.3). Thus given a spatial point x, the distribution of the mean value of $B(x)$, is highly non-Gaussian but the fluctuation of it in the neighborhood of radius $r \sim 1/k_s$ ($\ll 1/k_c$) has almost the same Gaussian nature as $A(x)_S/f$. This leads to $B_k \simeq B_* A_k/f$ for $k \gg k_c$.

For large scale ($k \ll k_c$), since small-scale fluctuations of $B(x)$ are irrelevant, a spatially averaged field should give the information of the fluctuation. We define such a field by

$$\bar{B}(x,r_a)=\frac{\int d^3y B(x-y)\theta(r_a-|x-y|)}{\int d^3y\,\theta(r_a-|x-y|)}\ , \tag{3.7}$$

where $\theta(x)$ is the step function and r_a is the averaging scale. In fact, this field is composed of the superposition of B_k satisfying $k \lesssim r_a^{-1}$. We note that $\bar{B}(x,|\eta|)=B(x)$ because of the ultraviolet cutoff at the horizon scale.

From Eq. (2.12), the two-point correlation damps exponentially beyond the correlation length $r_c=1/k_c$. As for the four-point correlation function, it also damps with the characteristic correlation length r_c (see Appendix A). Physically we expect that all the n-point correlations also damp with this characteristic length r_c in general. Thus for $r_a \gg r_c$, $\bar{B}(x,r_a)$ becomes an average of a large number of almost-independent probability variables. Therefore, from the central limit theorem, we expect that the probability distribution of $\bar{B}(x,r_a)$ will approach a Gaussian distribution. This mutual independence of $B(x)$ on large scale also explains the reason why the spectrum becomes white noise there as given by Eq. (2.14). On the other hand, for $r_a \ll r_c$, $\bar{B}(x,r_a)\simeq B(x)$, and the probability distribution of $\bar{B}(x,r_a)$ will approach Eq. (3.3).

B. Numerical model

For the intermediate scale ($k \sim k_c$) between the above two extreme cases, we numerically investigate the probability distribution. Our numerical method is based on an observation that a field configuration of $A(x,\eta)$ with fixed time η can be regarded as a Gaussian random process with a_k and $a_k^\dagger$ being the random-phase Gaussian probability variables. The detail is described in Appendix B. Then the baryon-number fluctuation $B(x)$ is calculated from Eq. (2.1). Calculation of the Fourier integral is done by using the fast Fourier transformation (FFT).

The ratio of the infrared cutoff and the ultraviolet cutoff, $N \equiv k_{\rm IR}/k_{\rm UV}$, is limited by the available number of grid points. Although we can generate the Fourier modes of $A(x)$ within $k_{\rm IR}<k<k_{\rm UV}$, the Fourier modes of $A(x)$ out of this range may be essential for those of $B(x)$ in $k_{\rm IR}<k<k_{\rm UV}$ due to the nonlinear nature of $B(x)$ in (2.1). In preliminary three-dimensional (3D) numerical simulations, we could not recover the power spectrum of the two-point correlation function of $B(x)$. This discrepancy was due to the lack of a sufficient number of grid points (in our present machine, only $N \sim 64$ is available). Therefore, in this section, we analyze a one-dimensional (1D) space model that supposedly preserves the essential features of the original 3D theory.

We take a 1D model in which the two-point correlation function of $A(x)$ has the same form as in the original 3D theory, i.e., (2.10). Since all the n-point correlation functions of the free field $A(z)$ are determined by the two-point function, all the correlation functions of $B(x)$ in the original theory can be reproduced in the 1D model by this prescription. In this sense, our 1D model is the same as analyzing the full 3D theory along a line.

The mode function $A_k^{(1)}$ in the 1D model can be read off from the integral form of the two-point correlation function of $A(x)$ in the 3D theory, Eq. (2.10). The in-

frared behavior ($k \to 0$) of A_k in Eq. (2.9) determines

$$|A_k^{(1)}| = \frac{H_*^{1+1/n}}{\sqrt{4\pi} k^{1/2+1/n}} . \tag{3.8}$$

It can be shown that this mode function in the 1D model (3.8) gives the two-point correlation function whose behavior is identical with that of $A(x)$ in the 3D theory (see Appendix C).

The spectrum of the fluctuations in the 1D model $P_B^{(1)}(k,\eta)$ is given by

$$\begin{aligned} P_B^{(1)}(k,\eta) &:= \int_{-\infty}^{+\infty} dx \langle B(x,\eta)B(0,\eta)\rangle e^{-ikx} \\ &= \frac{B_*^2}{k} e^{n\beta(\eta)} \int_0^\infty ds \cos s \exp\left[-\left[\frac{k_c}{k} s \right]^{2/n} \right] \\ &=: \frac{B_*^2}{k} e^{n\beta(\eta)} J^{(1)}(n,k) . \end{aligned} \tag{3.9}$$

Here we have defined a function $J^{(1)}(n,k)$ in analogy with Eq. (2.13). As in the 3D original theory, the function $J^{(1)}(n,k)$ has different asymptotic forms on the different sides of k_c, where the power spectrum $P_B^{(1)}(k,\eta)$ takes the form

$$P_B^{(1)}(k) \simeq \begin{cases} \dfrac{B_*^2 \pi}{kn} e^{n\beta(\eta)} \left[\dfrac{k}{k_c} \right]^{-2/n} & \text{for } k \gg k_c , \\ \dfrac{B_*^2}{k_c} e^{n\beta(\eta)} \Gamma\left[\dfrac{n}{2} + 1 \right] & \text{for } k \ll k_c . \end{cases} \tag{3.10}$$

Compared with Eq. (2.14), similar properties of the spectrum are also manifest in this model. Hence we expect that basic features of the fluctuation will be understood with this 1D model.

C. Numerical results

For the 1D model described in the above subsection, we have carried out simulations with $N = 10^5$. The power-law index of the scale factor has been taken to be $n = 6$. As a check of our numerical scheme, we have evaluated the two-point correlation function of $B(x)$ and its spectrum, and compared the numerical results with the analytic ones. We show the two-point correlation function in Fig. 1 and the spectrum in Fig. 2. As is seen there, our numerical scheme works well.

We have investigated the probability distribution $\rho(\bar{B}(x,r_a))$ as a function of $\bar{B}(x,r_a)$ defined by Eq. (3.7) for various values of the averaging scale r_a. The probability distribution is depicted in Figs. 3(a)–3(d) for several typical values of r_a in units of r_c. To exhibit the degree of deviations from the Gaussian distribution clearly, the horizontal axis is rescaled so that the variance is equal to unity, and the vertical axis is rescaled so that the area of each distribution function is unity. According to the numerical results, the probability distribution of $\bar{B}(x,r_a)$ changes its feature drastically when r_a crosses r_c.

In Fig. 2, we have indicated the wave number $k = 2\pi/r_a$ corresponding to each r_a of Figs. 3(a)–3(d). Comparing the averaging scale indicated in Fig. 2 with the corresponding distribution function, we find the distribution becomes Gaussian just when the power spectrum becomes white noise at $k \ll k_c$ or $r \gg r_c$. Vanishing of the correlation on large scale gives rise to the white-noise spectrum there. At the same time, it also makes the distribution Gaussian by the central limit theorem. The above picture was also confirmed in the case of the power indices of inflation $n = 4$ and $n = 8$.

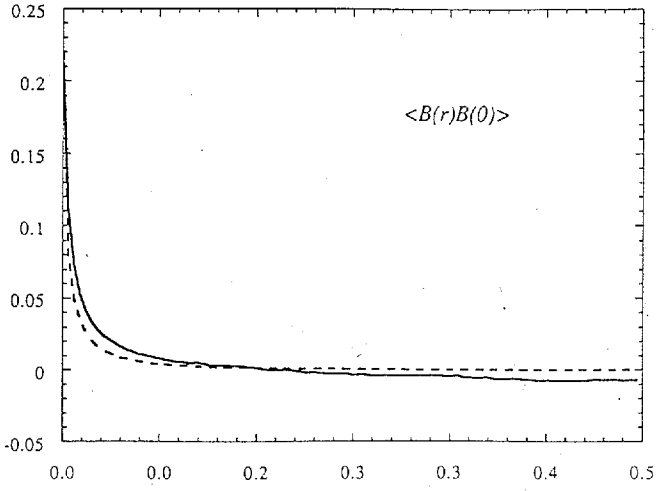

FIG. 1. Two-point correlation function of $B(x)$ in the 1D power-law inflation model. The model parameters are chosen as $n = 6$ and $\beta(\eta) = 0.01$. The dashed line is the analytic expression (2.12), and the solid line is the numerical result. The horizontal axis is normalized by the box size L, where the periodic boundary condition is imposed, and the vertical axis by B_*^2. The grid number is taken to be $N = 10^5$.

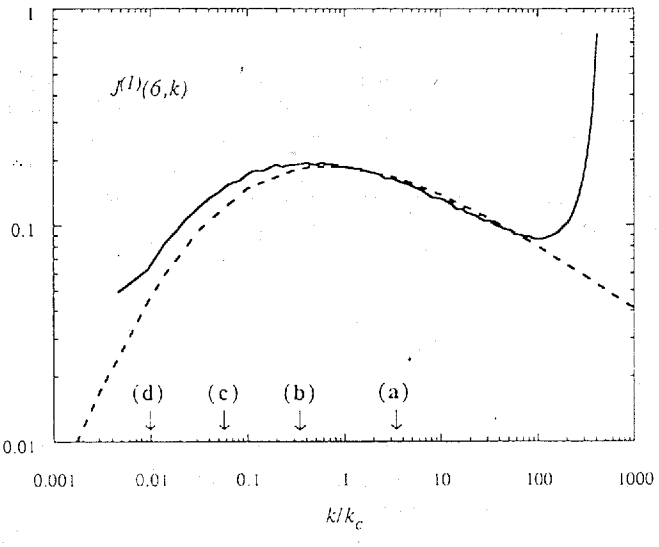

FIG. 2. Function $J^{(1)}(n,k)$ as a function of k/k_c. The model parameters are the same as in Fig. 1. The solid line is the result of the 1D Monte Carlo simulation, while the dashed line is that of numerical integration of Eq. (3.9). The large deviation at the high-frequency side is due to the finite-volume effect. The arrows (a)–(d) indicate the wave numbers corresponding to the averaging length scales of the probability distribution $\rho(\bar{B}(x,r_a))$ shown in Figs. 3(a)–(d).

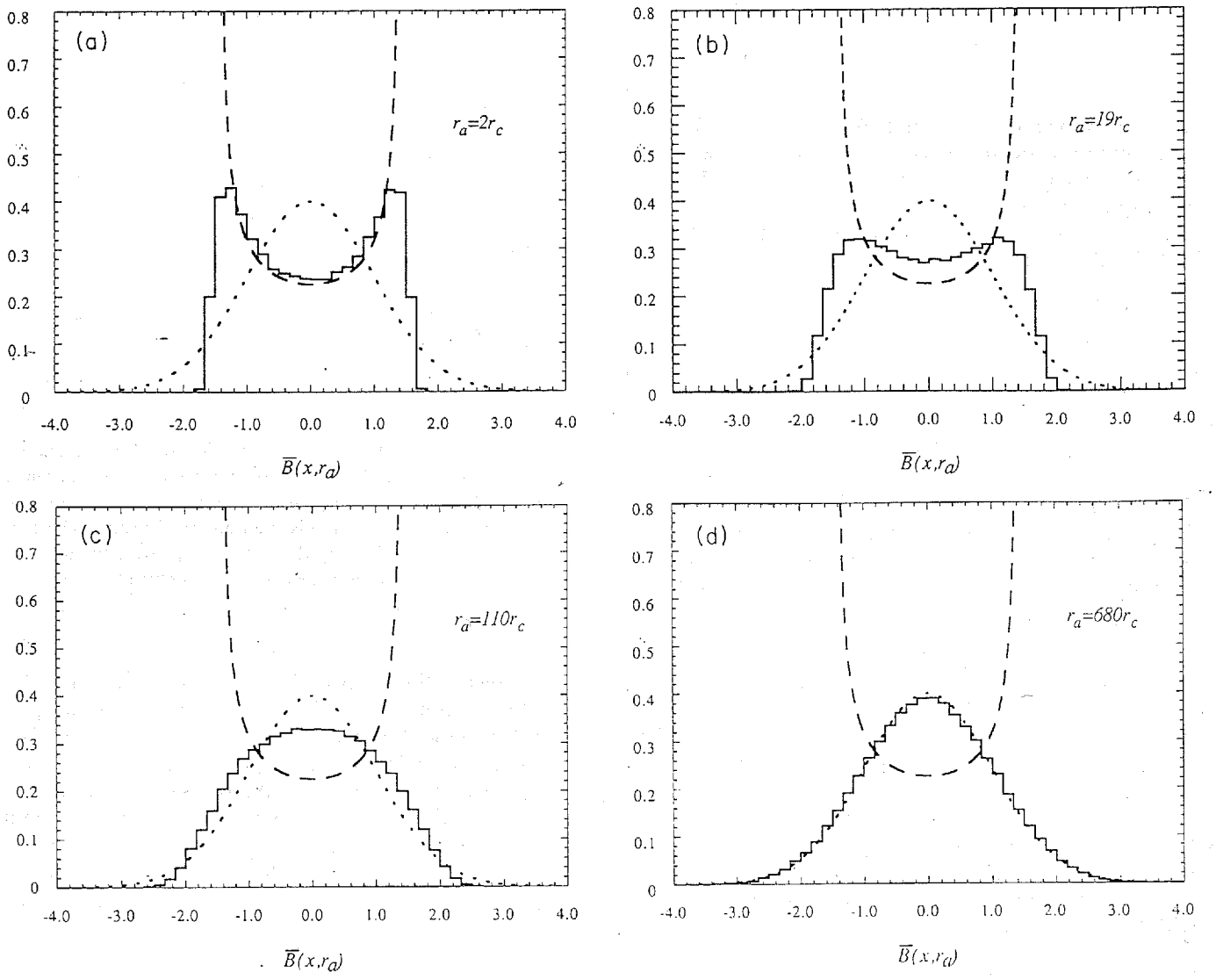

FIG. 3. Probability distribution $\rho(\bar{B}(x,r_a))$ of the baryon-number fluctuation averaged over the same r_a in the power-law inflationary background. The model parameters are the same as in Fig. 1. The averaging scale r_a is taken as (a) $r_a=2r_c$, (b) $19r_c$, (c) $110r_c$, and (d) $680r_c$. The horizontal axis is rescaled so that the variance is equal to unity. The actual variances are (a) $\sigma_B:=[\langle B(x)^2\rangle/B_*^2]^{1/2}=0.32$, (b) 0.16, (c) 0.059, and (d) 0.0012. The vertical axis is also rescaled so that the area of distribution function is unity. The dotted line in each figure shows the Gaussian distribution function that should be realized in the limit $r_a \gg r_c$, and the dashed line is the distribution function in the limit $r_a \ll r_c$, given by Eq. (3.3).

We have also investigated the probability distribution in the Fourier space. We have calculated the probability distributions of the real and imaginary parts of B_k. According to the numerical results, each B_k seems to behave just like a mutually independent random-phase Gaussian variable within the Poisson fluctuation of the numerical calculations, irrespective of the value of k. If B_k had the random-phase Gaussian distribution and if each B_k were independent, the probability distribution of $B(x)$ would have to be Gaussian too. This contradicts the result in the configuration space. Thus we conclude that the statement that each B_k is independent is wrong and the non-Gaussian properties are hidden in the higher-order correlations of B_k. In fact it is impossible to have $B(x)$ bounded

$$-B_* \le B(x)=\frac{1}{\sqrt{2\pi}}\int B_k e^{ikx}dk \le B_* \qquad (3.11)$$

without correlations among B_k's.

IV. PROBABILITY DISTRIBUTION IN PURE DE SITTER SPACE

A. Analytic properties

In the previous section, we have shown in terms of 1D numerical simulations that the statistical distribution becomes Gaussian on scale $k < k_c$ though the pointwise distribution of $B(x)$ is highly non-Gaussian. Here we present a complimentary analysis, namely, 3D simulations in the pure de Sitter background.

We note that the behavior of $A(x)$ and $B(x)$ has several different features in this space time compared with the case of power-law inflationary background. First, $B(x)$ has no characteristic scale such as k_c. Its power spectrum obeys a simple power law $|B_k|^2 \propto k^{-3+2\beta}$, as shown in Sec. II. Second, the fluctuations of $A(x)$ is scale invariant up to a logarithmic factor. Using the mode function (2.4), we find

$$\langle A(x)^2 \rangle = \frac{1}{(2\pi)^3} \int_{k_{\rm IR}}^{k_{\rm UV}} |A_k|^2 d^3k = \frac{H^2}{4\pi^2} \ln N , \quad (4.1)$$

where $N = k_{\rm UV}/k_{\rm IR}$. As before, the ultraviolet cutoff $k_{\rm UV}$ is naturally identified with the horizon scale: $k_{\rm UV} = 1/|\eta|$. On the other hand, the choice of the infrared cutoff $k_{\rm IR}$ depends on scales of one's interest. Fortunately, however, the dependence of $\langle A(x)^2 \rangle$ on $k_{\rm IR}$ is only logarithmic and hence relatively unimportant as long as $N \gg 1$ is satisfied. Thanks to these two properties, we may extract essential statistical information of $B(x)$ even if the dynamic range of a simulation is small. This allows us to perform a reliable fully 3D numerical simulation with relatively small N. In addition, we can easily generate various different realizations of the model by choosing various values of β.

From Eq. (3.1), the pointwise distribution is given by

$$\rho(B(x)) = \frac{1}{(B_*^2 - B^2)^{1/2}} \sum_{n \in Z} \frac{1}{\sqrt{2\pi}\sigma} \exp\left\{ -\frac{1}{2\sigma^2} \left[(-1)^n \arcsin\left[\frac{B}{B_*} \right] + n\pi \right]^2 \right\}, \quad \sigma := \sqrt{2\beta \ln N} . \quad (4.2)$$

For $\beta \ll 1$, it is almost Gaussian since we have $\sin[A(x)/f] \sim A(x)/f$. Hence $B(x)$ has the same statistical property as $A(x)$. On the other hand, for $\beta \sim 1$, $\rho(B)$ is highly non-Gaussian:

$$\rho(B(x)) = \frac{1}{\pi [B_*^2 - B^2(x)]^{1/2}} . \quad (4.3)$$

In this case, the power spectrum of B_k is steeper than the scale-invariant one; i.e., the spatial correlation damps more sharply as the length scale increases.

B. Numerical results

In this subsection we report the results of numerical simulations with particular emphasis on the scale dependence of the statistics. The method of simulations is the same as that in Sec. III (see Appendix B).

Simulations have been done on 128^3 grids in Fourier space, corresponding to $N = 128$. We have checked if we can reproduce the power spectrum $|B_k|^2$ for two cases of $\beta \ll 1$ and $\beta = 1$. In both of these cases, the power-law behavior $|B_k|^2 \propto k^{-3+2\beta}$ was verified except for a some deviation observed at $k < 20 k_{\rm IR}$ in the case of $\beta = 1$.

The pointwise probability distribution $\rho(B(x))$ for the case of $\beta = 10^{-3}$ is shown in Fig. 4, for $\beta = 0.02$ in Fig. 5(a), and for $\beta = 1$ in Fig. 6(a). The result for $\beta = 10^{-3}$ in Fig. 4 is consistent with the Gaussian distribution, as expected. On the other hand, in the other two cases, $\rho(B(x))$ exhibits a strongly non-Gaussian feature. These results agree with the analytic formula we have estimated in the previous subsection. For comparison, we have also done simulations with $N = 64$ but found no measurable difference in the results. This justifies our expectation that a reliable simulation can be done in the case of pure de Sitter background, even with a relatively small N.

As in Sec. III, we have calculated the distribution function of the volume-averaged field on scale r_a, $\rho(\bar{B}(x, r_a))$. The results are shown for $\beta = 0.02$ in Figs. 5(b) and 5(c), with $r_a = 5|\eta|$ and $r_a = 20|\eta|$, respectively, and for $\beta = 1$ in Fig. 6(b) with $r_a = 2|\eta|$. Interestingly, as the averaging scale r_a is increased, the distribution function $\rho(\bar{B}(x, r_a))$ approaches the Gaussian distribution more rapidly in the case of $\beta = 1$, for which the non-Gaussian feature is originally stronger, than in the case of $\beta = 0.02$.

This result can be understood by considering the higher-order correlation functions of $B(x)$, which can be estimated by the procedure similar to Appendix A. We find the $2m$-point correlation function in de Sitter space time as

$$\left\langle \prod_{j=1}^{2m} B(x_j) \right\rangle \simeq \left[\frac{B_*^2}{4} \right]^m \left[\frac{\eta^2}{r_{\rm avg}^2} \right]^{m\beta} , \quad (4.4)$$

where $r_{\rm avg}$ denotes a typical length of separation between x_j's. Thus the higher-order correlations of $B(x)$ decrease more rapidly as $r_{\rm avg}$ is increased and the rate is faster for larger β. This explains why the spatially averaged field

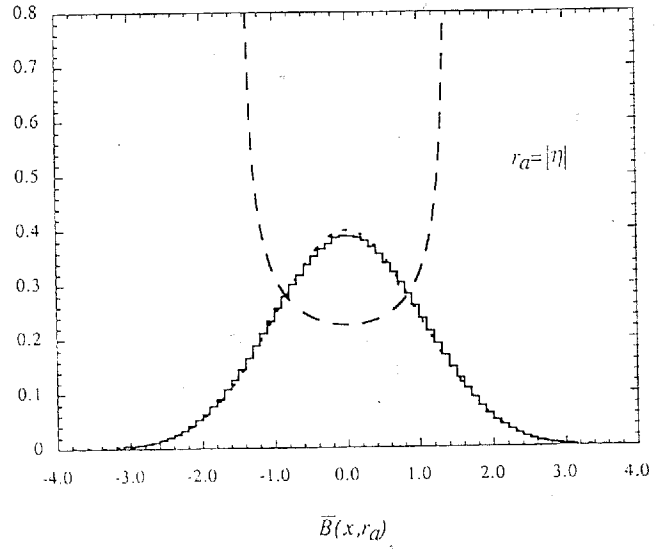

FIG. 4. Probability distribution of $B(x)$ in the pure de Sitter universe, which is equivalent to $\bar{B}(x, r_a)$ with $r_a = |\eta|$. The model parameter is $\beta = 10^{-3}$. The grid number is $N^3 = 128^3$. The normalizations of the horizontal and vertical axes are the same as in Fig. 3. The actual variance is $\sigma_B = 0.324$.

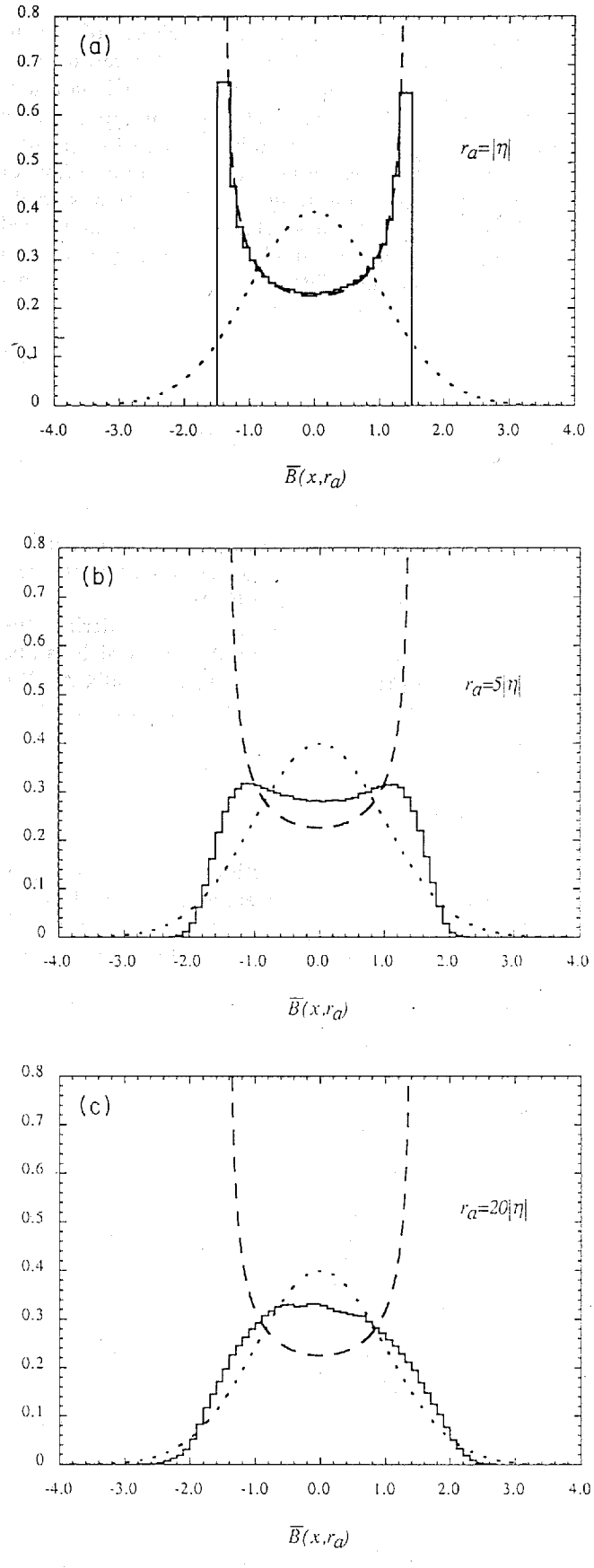

FIG. 5. Probability distribution of $\bar{B}(x,r_a)$ in the pure de Sitter universe with $\beta=0.02$. The averaging scale r_a is taken as (a) $r_a=|\eta|$, (b) $5|\eta|$, and (c) $20|\eta|$. Note that $\bar{B}(x,|\eta|)=B(x)$. The actual variances are (a) $\sigma_B=0.701$, (b) 0.382, and (c) 0.198.

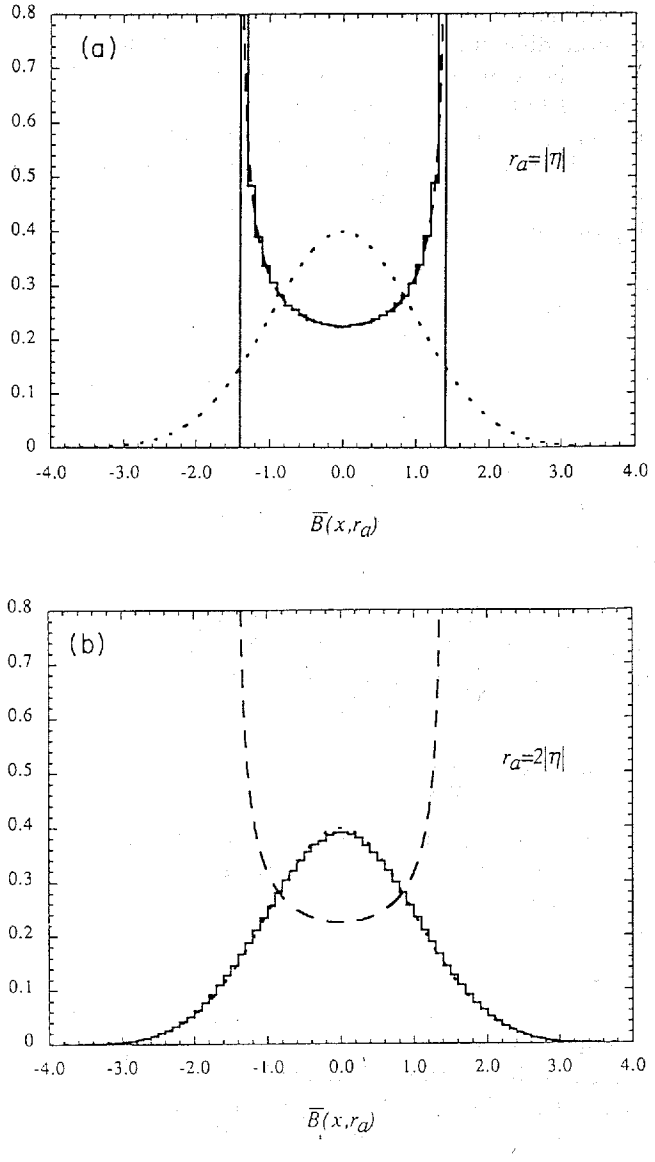

FIG. 6. Same as Fig. 5, but with $\beta=1$. The averaging scale r_a is taken as (a) $r_a=|\eta|$ and (b) $2|\eta|$. The variances are (a) $\sigma_B=0.707$ and (b) 0.250.

approaches a Gaussian random field faster for $\beta=1$ than for $\beta=0.02$.

On the other hand, for $\beta\ll 1$, the fluctuation of $B(x)$ is intrinsically Gaussian as discussed previously. Therefore the baryon-number fluctuation in the pure de Sitter universe is always Gaussian on scales beyond a few horizon lengths in the inflationary era, and consequently on any scale of astrophysical importance.

V. DISCUSSION AND CONCLUSION

In the present paper, we have investigated the nature of probability distribution of the baryon-number fluctuation $B(x)$ generated at the inflationary era of the universe, which is a sinusoidal function of a free massless field $A(x)$.

In addition to analytical investigations that we have done for some limiting cases, we have carried out numeri-

cal simulations to clarify the statistical properties of the baryon-number fluctuation. Simulations have been done by the Monte Carlo method, based on the observation that the quantum field $A(x)$ on a fixed spacelike hypersurface can be regarded as a random Gaussian field.

For the baryon-number fluctuation associated with power-law inflation, we have considered a 1D model in place of the original 3D theory, in order to realize a sufficiently wide dynamic range of Fourier modes. Our 1D model preserves all the essential features of the original theory such as the n-point correlation functions. We have calculated the probability distribution on various scales in the configuration space.

We have found on small scale ($k \gg k_c$), where the baryon-number spectrum is almost scale invariant, the distribution is highly non-Gaussian. Since it is peaked near at the maximum possible value of $|B(x)|$, this model may result in efficient formation of pregalactic stars, which is desirable for the minimal isocurvature scenario in which reionization of the medium is presumed.

On the other hand, on large scale ($k \ll k_c$), where the spectrum approaches white noise, the baryon-number fluctuation is Gaussian. Thus the predicted amplitude of the large-angle CMB anisotropy calculated by various authors, which is based on the Gaussian statistics and which imposes presently the most stringent constraint on baryon isocurvature models, is applicable to our model as well.

For comparison and completeness we have also calculated the probability distribution for a fully 3D model, but in the pure de Sitter background. Interestingly, it shows a very different behavior from the case of power-law inflation. In fact, the distribution rapidly becomes Gaussian as the averaging length exceeds $\sim 20H^{-1}$. This is because in the pure de Sitter space time each logarithmic interval of length scale gives the same contribution to the fluctuation of $A(x)$ and it is ultraviolet divergent without a cutoff. Hence the higher-order correlation functions decrease rapidly as the averaging scale increases.

On the contrary, since the fluctuation of $A(x)$ is ultraviolet finite in the power-law inflationary background, the volume-averaged fluctuation of $B(x)$ is dominated by large-scale modes. Thus it is not until the power spectrum becomes white noise that the distribution becomes Gaussian.

As is seen above, exponential inflation and power-law inflation have very different predictions on the statistical properties of the baryon-number fluctuations. We plan to clarify if it is a generic feature using various functions other than $B(x)$.

ACKNOWLEDGMENTS

K.Y. would like to thank S. Mizoguchi for discussion. H.S. acknowledges JSPS for financial support. J.Y. acknowledges JSPS for supporting his visit to Fermilab, where part of the work was done. This work was supported in part by the Japanese Grant-in-Aid for Scientific Research Fund of the Ministry of Education, Science, and Culture, No. 02640231.

APPENDIX A

In this appendix, we derive a general form of the equal-time $2m$-point correlation function [17] of $B(x)$ in the power-law inflationary background and show that in addition to the two-point function, the four-point function also damps with the characteristic length r_c.

Using $\sin x = (e^{ix} - e^{-ix})/(2i)$, the $2m$-point function of $B(x)$ can be written as

$$\left\langle \prod_{j=1}^{2m} B(x_j) \right\rangle = \left[\frac{B_*^2}{-4} \right]^m \sum_{\sigma} \left[\prod_{j=1}^{2m} \sigma_j \right] \left\langle \exp\left[i \sum_{j=1}^{2m} \sigma_j A(x_j)/f \right] \right\rangle , \tag{A1}$$

where σ_j takes the value $+1$ or -1, and the summation is taken over all the combinations of $\sigma \equiv (\sigma_1, \sigma_2, \ldots, \sigma_{2m}) \in (\pm 1, \pm 1, \ldots, \pm 1)$. For the right-hand side, we have

$$\left\langle \exp\left[i \sum_{j=1}^{2m} \sigma_j A(x_j)/f \right] \right\rangle = \exp\left[-\tfrac{1}{2} \sum_{j,k} \sigma_j \sigma_k \langle A(x_j) A(x_k)/f^2 \rangle \right] \tag{A2}$$

by taking the source function of $A(x)$ as $j(x) = i \sum_{j=1}^{2m} \sigma_j \delta(x - x_j)/f$ [12]. In particular, the two-point function of $A(x)$ is given by Eq. (2.10):

$$\langle A(x_j) A(x_k)/f^2 \rangle \simeq n\beta \left[\left[\frac{r_0^2}{\eta^2} \right]^{1/n} - \left[\frac{r_{jk}^2}{\eta^2} \right]^{1/n} \right] \equiv g(r_0) - g(r_{jk}) , \tag{A3}$$

where we have abbreviated $\beta(\eta)$ as β and defined $g(r) := n\beta (r^2/\eta^2)^{1/n}$ and $r_{jk} := |x_j - x_k|$. By separating the summation in the right-hand side of Eq. (A2) to $j = k$ and $j \neq k$, we have

$$\left\langle \prod_{j=1}^{2m} B(x_j) \right\rangle \simeq \left[\frac{B_*^2}{-4} \right]^m \sum_{\sigma} \left[\prod_{j=1}^{2m} \sigma_j \right] \exp\left[- \left[\sum_{j<k} \sigma_j \sigma_k + m \right] g(r_0) + m g(|\eta|) + \sum_{j<k} \sigma_j \sigma_k g(r_{jk}) \right] , \tag{A4}$$

where we have set $g(r_{jj})=g(|\eta|)$ since $|\eta|$ is the ultraviolet cutoff in this model. For a sufficiently large r_0, we have $g(r_0)\gg 1$. Hence only the combinations of σ that satisfy

$$\sum_{j<k}\sigma_j\sigma_k \le -m \tag{A5}$$

will contribute to the correlation function of $B(x)$ in Eq. (A4). However it can be shown that for all possible combinations of σ, we have $\sum_{j<k}\sigma_j\sigma_k \ge -m$ and the equality holds only for a combination of σ with $\sum_{j=1}^{2m}\sigma_j=0$, i.e., a mixture of equal numbers of $+1$ and -1. Thus Eq. (A4) reduces to

$$\left\langle \prod_{j=1}^{2m} B(x_j)\right\rangle \simeq \left[\frac{B_*^2 e^{n\beta}}{4}\right]^m \times {\sum_{\sigma}}' \exp\left[n\beta \sum_{j<k}\sigma_j\sigma_k\left[\frac{r_{jk}^2}{\eta^2}\right]^{1/n}\right], \tag{A6}$$

where the prime means the summation is taken only over the combinations of σ with $\sum_{j=1}^{2m}\sigma_j=0$. Note that the dependence on the infrared cutoff r_0 disappears in the correlation function of $B(x)$.

For the two-point function ($m=1$), Eq. (A6) gives

$$\langle B(x_1)B(x_2)\rangle \simeq \frac{B_*^2 e^{n\beta}}{2}\exp\left[-n\beta\left[\frac{r_{12}^2}{\eta^2}\right]^{1/n}\right], \tag{A7}$$

and this exponentially damps with the characteristic length $r_c:=|\eta|/(n\beta)^{n/2}$.

For a general m, if the exponent in Eq. (A6) is shown to be negative definite for any configuration of x_j, we may expect that

$$\sum_{j<k}\sigma_j\sigma_k\left[\frac{r_{jk}^2}{\eta^2}\right]^{1/n} \simeq -m\left[\frac{r_{\rm avg}^2}{\eta^2}\right]^{1/n}, \tag{A8}$$

and all the $2m$-point functions dump with a length scale that is of the same order of r_c. Here $r_{\rm avg}$ is an average length of r_{jk}'s, and the factor m arises from the difference between the number of combinations of (j,k) with $\sigma_j\sigma_k=-1; m^2$, and that of (j,k) with $\sigma_j\sigma_k=1; {}_{2m}C_2=m(m-1)$. Although the negativity of the exponent in Eq. (A6) is physically reasonable (otherwise the correlation will diverge when the system is scaled up), we have not yet found a convincing proof for this [18].

For the four-point function we can show the negativity of $\sum_{j<k}\sigma_j\sigma_k r_{jk}^{2/n}$ as follows. In this case, Eq. (A6) gives

$$\begin{aligned}\langle B(x_1)B(x_2)B(x_3)B(x_4)\rangle \simeq 2\left[\frac{B_*^2 e^{n\beta}}{4}\right]^2 \Bigg\{ &\exp\left[-\frac{n\beta}{\eta^{2/n}}(r_{12}^{2/n}+r_{13}^{2/n}-r_{14}^{2/n}-r_{23}^{2/n}+r_{24}^{2/n}+r_{34}^{2/n})\right] \\ &+\exp\left[-\frac{n\beta}{\eta^{2/n}}(r_{12}^{2/n}-r_{13}^{2/n}+r_{14}^{2/n}+r_{23}^{2/n}-r_{24}^{2/n}+r_{34}^{2/n})\right] \\ &+\exp\left[-\frac{n\beta}{\eta^{2/n}}(-r_{12}^{2/n}+r_{13}^{2/n}+r_{14}^{2/n}+r_{23}^{2/n}+r_{24}^{2/n}-r_{34}^{2/n})\right]\Bigg\}.\end{aligned} \tag{A9}$$

Now, we write the exponent of the first term in the right-hand side of Eq. (A9) as

$$\begin{aligned}&-(r_{12}^{2/n}+r_{13}^{2/n}-r_{14}^{2/n}-r_{23}^{2/n}+r_{24}^{2/n}+r_{34}^{2/n}) \\ &\quad=-\tfrac{1}{2}[(r_{12}^{2/n}+r_{13}^{2/n}-r_{23}^{2/n})+(r_{13}^{2/n}+r_{34}^{2/n}-r_{14}^{2/n}) \\ &\qquad+(r_{12}^{2/n}+r_{24}^{2/n}-r_{14}^{2/n})+(r_{24}^{2/n}+r_{34}^{2/n}-r_{23}^{2/n})].\end{aligned} \tag{A10}$$

Then we can use the triangle inequality on flat space; $r_{12}+r_{13}\ge r_{23}$, etc., to show the non-negativity of the terms in the square brackets: $r_{12}^{2/n}+r_{13}^{2/n}-r_{23}^{2/n}\ge 0$, etc. The same logic can be applied to the other exponents in Eq. (A9), and it is easily seen that the equalities cannot hold simultaneously for any configuration of x_j $(j=1,2,3,4)$. This implies $\sum_{j<k}\sigma_j\sigma_k r_{jk}^{2/n}<0$ for $m=2$. It is then naturally expected that the four-point function damps with a characteristic length of order r_c. For example, if we choose $r_{12}=r_{13}=r_{23}=r_1$ and $r_{14}=r_{24}=r_{34}=r_2$, then the above four-point correlation function reduces to a product of the two-point functions:

$$\langle B(x_1)B(x_2)B(x_3)B(x_4)\rangle = \tfrac{3}{2}\langle B(r_1)B(0)\rangle\langle B(r_2)B(0)\rangle. \tag{A11}$$

APPENDIX B

In this appendix, we show that the *equal-time* distribution of a free field $A(x,\eta)$ can be interpreted as a Gaussian random process, in which the creation and annihilation operators of $A(x,\eta)$ are regarded as the random-phase Gaussian probability variables. Our Monte Carlo simulations are based on this observation.

For our purpose, we start with a free scalar field $A(x,\eta)$ in q-dimensional flat space, normalized in a box $0\le x_i\le L$ $(i=1,\ldots,q)$ with periodic boundary conditions

$$A(x,\eta) = \sum_{m_1=-\infty}^{+\infty}\cdots\sum_{m_q=-\infty}^{+\infty}\frac{1}{L^{q/2}}[\hat{a}_{k_m}A_{k_m}(\eta)\times\exp(ik_m x)+\text{H.c.}], \tag{B1}$$

where $x=(x_1,\ldots,x_q)$, $k_m=2\pi(m_1,\ldots,m_q)/L$, and $[\hat{a}_{k_m},\hat{a}^{\dagger}_{k_{m'}}]=\delta_{k_m,k_{m'}}$.

We consider a generating functional [17] for the equal-time correlation functions

$$Z[j;\eta]=\left\langle \exp\left[\int_0^L d^q x\ A(x,\eta)J(x)\right]\right\rangle . \tag{B2}$$

In terms of the mode decomposition (B1), the above expression reads

$$Z[j;\eta]=\left\langle \exp\left[\sum_m (\hat{a}_{k_m} A_{k_m}(\eta) j^*_{k_m} + \text{H.c.})\right]\right\rangle , \tag{B3}$$

where

$$j_{k_m} := \frac{1}{L^{q/2}} \int_0^L d^q x\ j(x)\exp(-ik_m x) . \tag{B4}$$

On the other hand, using the fact that $A(x,\eta)$ is a free field, i.e., the action is quadratic in $A(x,\eta)$, Eq. (B2) is evaluated as

$$\begin{aligned} Z[j;\eta] &= \exp\left[\tfrac{1}{2}\int_0^L d^q x\, d^q y\, j(x)\langle A(x,\eta)A(y,\eta)\rangle j(y)\right] \\ &= \exp\left[\tfrac{1}{2}\sum_m |A_{k_m}(\eta) j_{k_m}|^2\right] . \end{aligned} \tag{B5}$$

Then we take a product of Eq. (B5) and unity:

$$1=\int \prod_m \left[\frac{dz_m dz_m^*}{\pi i}\right] \exp\left[-2\sum_m |z_m|^2\right] , \tag{B6}$$

where the integration measure $dz\,dz^*/\pi i$ means $2\,du\,dv/\pi$ with $z=u-iv$. If we shift the integration variables as

$$z_m \to z_m - \tfrac{1}{2} A^*_{k_m}(\eta) j_{k_m} , \tag{B7}$$

Eq. (B5) is rewritten in the form

$$\begin{aligned} Z[j;\eta] = \int \prod_m \left[\frac{dz_m dz_m^*}{\pi i}\right] &\exp\left[-2\sum_m |z_m|^2\right] \\ &\times \exp\left[\sum_m (z_m A_{k_m}(\eta) j^*_{k_m} + \text{c.c.})\right] . \end{aligned} \tag{B8}$$

Comparison of Eqs. (B3) and (B8) shows that all the equal-time correlation functions are reproduced by the replacements

$$\begin{aligned} &a_{k_m} \to z_m , \\ &a^\dagger_{k_m} \to z^*_m , \\ &\langle \{\cdots\}\rangle \to \int \prod_m \left[\frac{dz_m dz_m^*}{\pi i}\right] \exp\left[-2\sum_m |z_m|^2\right] \{\cdots\} . \end{aligned} \tag{B9}$$

With the above interpretation, we can regard a configuration of the field $A(x)$ as a Gaussian random process. Finally, if we set $z_m = r_m e^{i\theta_m}$, the probability measure in Eq. (B9) is rewritten as

$$\frac{e^{-2|z_m|^2}}{\pi i} dz_m dz_m^* = \frac{e^{-2r_m^2}}{\pi} dr_m^2 d\theta_m . \tag{B10}$$

Thus the above demonstration shows that $A(x)$ has the random-phase Gaussian distribution.

APPENDIX C

In this appendix, we estimate the two-point correlation function of $A^{(1)}(x)$ in the 1D model, where the mode function is given by Eq. (3.8). Like Eq. (2.3) we expand $A^{(1)}(x,\eta)$ as

$$\begin{aligned} A^{(1)}(x,\eta) = \int \frac{dk}{(2\pi)^{1/2}} [&\hat{a}_k^{(1)} A_k^{(1)}(\eta)\exp(ikx) \\ &+ \hat{a}_k^{(1)\dagger} A_k^{(1)}(\eta)^*\exp(-ikx)] , \end{aligned} \tag{C1}$$

where x and k are one dimensional. Then the two-point correlation function of $A^{(1)}(x,\eta)$ is calculated as

$$\begin{aligned} \langle A^{(1)}(r)A^{(1)}(0)\rangle &= \frac{1}{2\pi}\int_{1/r_0}^{1/|\eta|} dk\, |A_k^{(1)}|^2 2\cos(kr) \\ &= \frac{H_*^{2+2/n}}{4\pi^2} \int_{1/r_0}^{1/|\eta|} dk \frac{\cos(kr)}{k^{1+2/n}} , \end{aligned} \tag{C2}$$

where r_0^{-1} and $|\eta|^{-1}$ are the infrared and ultraviolet cutoffs, respectively. Integration by parts of Eq. (C2) yields

$$\begin{aligned} (\text{C2}) &= \frac{H_*^{2+2/n}}{4\pi^2} \left\{ \left[-\frac{n}{2} k^{-2/n}\cos kr \right]_{1/r_0}^{1/|\eta|} \right. \\ &\qquad \left. - \frac{n}{2} r \int_{1/r_0}^{1/|\eta|} dk\, k^{-2/n}\sin kr \right\} \\ &\simeq \frac{H_*^{2+2/n}}{4\pi^2} r^{2/n} \left[\frac{n}{2} \left[\frac{r}{r_0}\right]^{-2/n} - \frac{n}{2} \right] \\ &\simeq n\beta(\eta) \left[\left[\frac{r_0^2}{\eta^2}\right]^{1/n} - \left[\frac{r^2}{\eta^2}\right]^{1/n} \right] \end{aligned} \tag{C3}$$

This is in the same form as Eq. (2.10). The procedure to find the n-point correlation of $B(x)$ from the two-point correlation function of $A(x)$ is just the same as in the 3D case. Thus the n-point correlation function of $B(x)$ has the same form as that of the full 3D theory.

[1] P. J. E. Peebles and J. Silk, Nature **346**, 233 (1990).

[2] K. Sato, Mon. Not. R. Astron. Soc. **195**, 467 (1981); A. H. Guth, Phys. Rev. D **23**, 347 (1981).

[3] Y. Suto and T. Suginohara, Astrophys. J. Lett. **370**, L15 (1991).

[4] M. J. Geller and J. P. Huchra, Science **246**, 897 (1989); W. Saunders *et al.*, Nature **349**, 32 (1991).

[5] G. F. Smoot, *et al.*, Astrophys. J. Lett. **396**, L1 (1992).

[6] P. J. E. Peebles, in *The Early Universe*, edited by W. G. Unruh and G. W. Semenoff (Reidel, Dordrecht, 1988), p. 203; Astrophys. J. Lett. **315**, L73 (1987); Nature **327**, 210 (1987); in *Large Scale Structure and Motions in the Universe*, Proceedings of the Meeting, Trieste, Italy, 1988, edited by M. Mezzetti *et al.* (Kluwer, Dordrecht, 1989), p.

119.
[7] J. A. Tyson, Astron. J. **96**, 1 (1988); M. Fukugita, F. Takahara, K. Yamashita, and Y. Yoshii, Astrophys. J. Lett. **361**, L1 (1990).
[8] K. Sato, in *Proceedings of the IUPAP Conference on Primordial Nucleosynthesis and Evolution of the Early Universe,* Tokyo, 1990, edited by K. Sato and J. Audouze (Kluwer, Dordrecht, 1991), p. 79.
[9] J. R. Bond, G. Efstathiou, P. M. Lubin, and P. R. Meinhold, Phys. Rev. Lett. **66**, 2179 (1991).
[10] J. Yokoyama and Y. Suto, Astrophys. J. **379**, 427 (1991).
[11] T. Suginohara and Y. Suto, Astrophys. J. **387**, 431 (1992).
[12] M. Sasaki and J. Yokoyama, Phys. Rev. D **44**, 970 (1991).
[13] L. F. Abbott and M. B. Wise, Nucl. Phys. **B244**, 541 (1984); F. Lucchin and S. Matarrese, Phys. Rev. D **32**, 1316 (1985).
[14] D. La and P. J. Steinhardt, Phys. Rev. Lett. **62**, 376 (1989); A. L. Berkin, K. Maeda, and J. Yokoyama, Phys. Rev. Lett. **65**, 141 (1990).
[15] M. Yoshimura, Phys. Rev. Lett. **51**, 439 (1983).
[16] M. Sasaki and B. L. Spokoiny, Mod. Phys. Lett. A **6**, 2935 (1991).
[17] Throughout this paper, we interpret a multipoint correlation function as a vacuum expectation value of the *totally symmetric* product of the operators. For example,

$$\langle B(x_1)B(x_2)\rangle \equiv [\langle B(x_1)B(x_2)\rangle + \langle B(x_2)B(x_1)\rangle]/2 \ .$$

This interpretation may be regarded as the equal-time limit of the time-ordered product and it enables us to reinterpret the system in a statistical language as in Appendix B.
[18] We examined this conjecture by generating random configurations of x_j's numerically. For $m=3-1000$, we did not find any counterexample of this conjecture. We thank Y. Suto for setting this numerical experiment.